Lamination Surface Defects in Composites

Amrit Poudel

Materials Processing Technology (English)

2019

DEGREE THESIS	
Arcada	
Degree Programme:	Materials Processing Technology
Identification number:	20393
Author:	Amrit Poudel
Title:	Lamination Surface Defects in Composites
Supervisor (Arcada):	Rene Herrmann

Abstract:

The manufacturing process of composites depends upon different factors. Fluctuation on those factors may leads to various defects on the product. Those defects can be seen on the surface of the composites. This thesis scope was to study the defects on the surface of laminate composites. The aim of this study was to study the surface defects through optical microscope and quantify the defects with analyzing their geometry and to find out how much the defects reduce the strength of specimens. Glass fiber with density of 2540kg/m^3 and ATLAC E-Nova 6215 Vinyl ester resin with density 1140kg/m^3 was used to manufacture laminate composites. Two fiber sheets represented as 'A' and 'B' were used with fabric orientation of 0/90/m70 and +45/-45/m100. Thirty different samples, grouped as ABA and BAB symmetric were used for the study. Samples were cut into length of 180mm per piece. Width of samples ABA symmetric ranged from 15.10mm to 15.20mm with thickness ranged from 5.25mm to 5. 60mm.Whereas, width of BAB symmetric samples ranged from 15.00mm to 15.15mm with thickness of 4mm to 4. 30mm.The surface of samples was analyzed on the microscope which helped to detect defects on samples. Air bubbles with diameter from 10micron to100 micron respectively were detected on samples. Using the dimension and analyzing the geometry of defect calculation was done to find the stress concentration factor around the defects which gave value of 3 for all defects.

Testometric machine was used for 3-point bending test from where the experimental data for flexural modulus was collected. Experimental flexural modulus for samples BAB symmetric ranged from 20425.73MPa to 22971.34MPa, whereas for sample ABA symmetric the value ranged from 22638.30MPa to 28921.57MPa. Composite Compressive Strength Modeller(CCSM) calculator was used to calculate the theoretical stiffness of the samples. The calculation gave flexural modulus for BAB symmetric samples ranged from 23714MPa to 26360MPa, whereas for ABA symmetric sample the value ranged from 289130MPa to 30605MPa. The data obtained from both of the calculation were compared. The sample with higher number of defects had the lowest experimental strength where the difference between experimental and theoretical strength was 5294.64MPa (BAB symmetric samples),7265.03MPa (ABA symmetric samples). The lowest difference of values was 2359.65MPa for BAB symmetric sample and 1683.43MPa for ABA symmetric samples. Both sample had lesser number of defects.

Keywords:	Surface Defects, Hooke's law,Stress Concentration,Fracture Mechanics, 3-point bending,Microscope analysis,CCSM calculation
Number of pages:	39
Language:	English
Date of acceptance:	

Table of Contents

Tables

1 Introduction

1.1 Background

Humans have master the use of various materials to make our life more easy and comfortable. There is long history of us inventing new materials and developing them in our conventional way. Composites are among those which has brought big revolution on modern material science. When two materials with different properties are mixed the new material is formed with different physical and chemical properties called composites. Laminated Composites have shown the possibilities to replace metals and other traditional materials. Despite of having many advanced features, there are still some problems related with them. The manufacture processing of the composites depends upon the different factors like pressure, temperature, orientation of fibers, quality of resin etc. When something goes wrong with any of the processing factors, various defects can be seen on the product [1]. One of those defects which can see on the laminated composites are air bubbles or voids on the surface, define as term surface defects. In spite of being light weight, they are known for high strength and stiffness. Surface defects on the composites may bring changes on the mechanical properties of the product and decrease its sustainability. So, it's important that the product doesn't possess those defects. Even a small hole on the surface can grow to form a crack which propagates to certain point to form fracture on a structure.

1.2 Objectives

This study aims to analyze surface defects through optical microscope and study how the surface defects behave, their geometry, where do they exist and its effect on the mechanical properties of the composites. 3-point bending test will be done to compare the bending modulus of the defect sample with an ideal one. The study purpose to find how the defects change the quality of the surface. The defects can be quantified in terms of the defect geometry, helping to calculate stress concentration. The stress concentration leads to decrease in the sustainability of the product or even material failure. The defects on the surface of our laminate composite will be active catalyst for stress concentration. Having numbers of those defects will leads to uneven distribution of stress throughout the whole-body structure and the consequences can be catastrophic. The stress concentration changes the strength of the specimen. Using this existed theory this thesis aims to study the impact of defects on the strength of the tested specimen.

2 Literature Review

2.1 Hooke's Law

Hooke's law of elasticity states that for relatively small deformation of an object, the size of deformation is directly proportional to deforming force. Mathematically the law can be expressed as,

$$F = kx \qquad \textit{eqn 2-1}$$

Where, F is the applied force

x is the displacement due to force

k is the constant (elastic modulus) depends on the kind of elastic material and their geometry

After the force is removed the elastic material return to its original form. When the applied force is relatively large the displacement is expected to be larger as well, according to Hooke's law [2].The different stages of material under the load can be seen on the stress-strain curve,

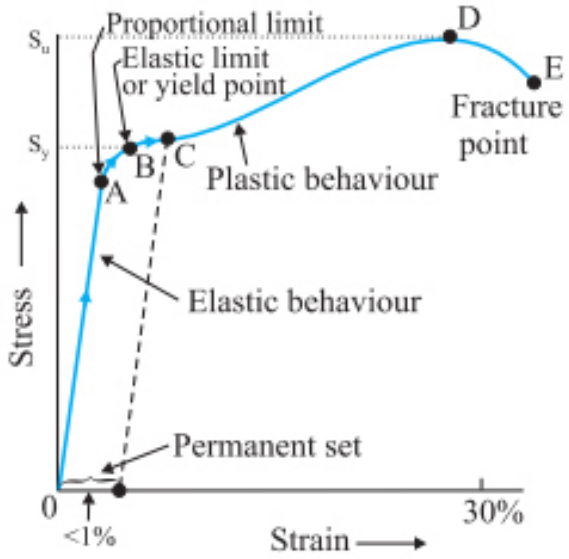

Figure 2.1 Stress-Strain Curve [3]

2.2 Stress Concentration

Stress distribution is not always uniform as the cross-section of the structural material varies. The body may contain cracks, holes, notches, sharp corners and so forth due to which the intensity of stress get directed in those specific areas. [4]

Stress Concentration is also known as stress raiser. The stress raiser effect can be calculate using theoretical method, stress concentration factor(K_t) given as [5]

$$\sigma_{max} = K_t \sigma_{ave} \qquad \textit{eqn 2-2}$$

$$K_t = \sigma_{max}/\sigma_{ave}$$

where σ_{max} is maximum stress applied on the body, σ_{ave} is reference stress

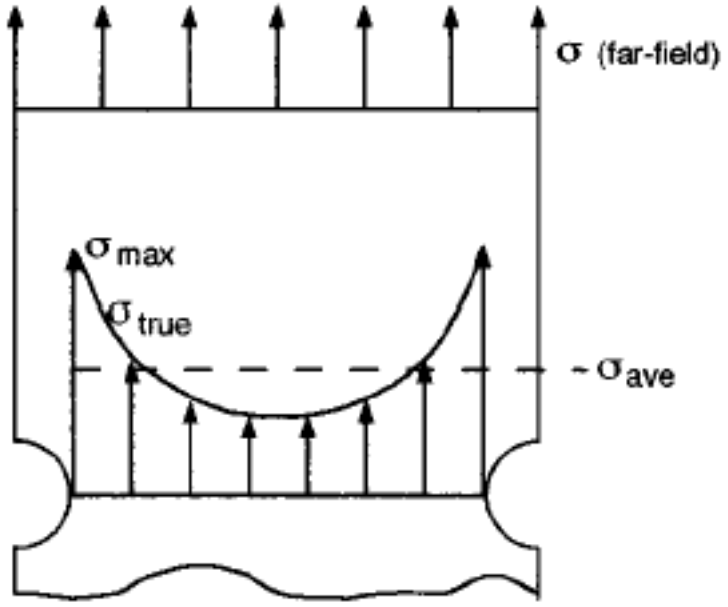

Figure 2.2 Stress Distribution in notched area under unidirectional load [5]

The stress concentration factor depends upon the geometry of notches and cracks.

2.2.1 Nominal Stress and Stress Concentration around Hole

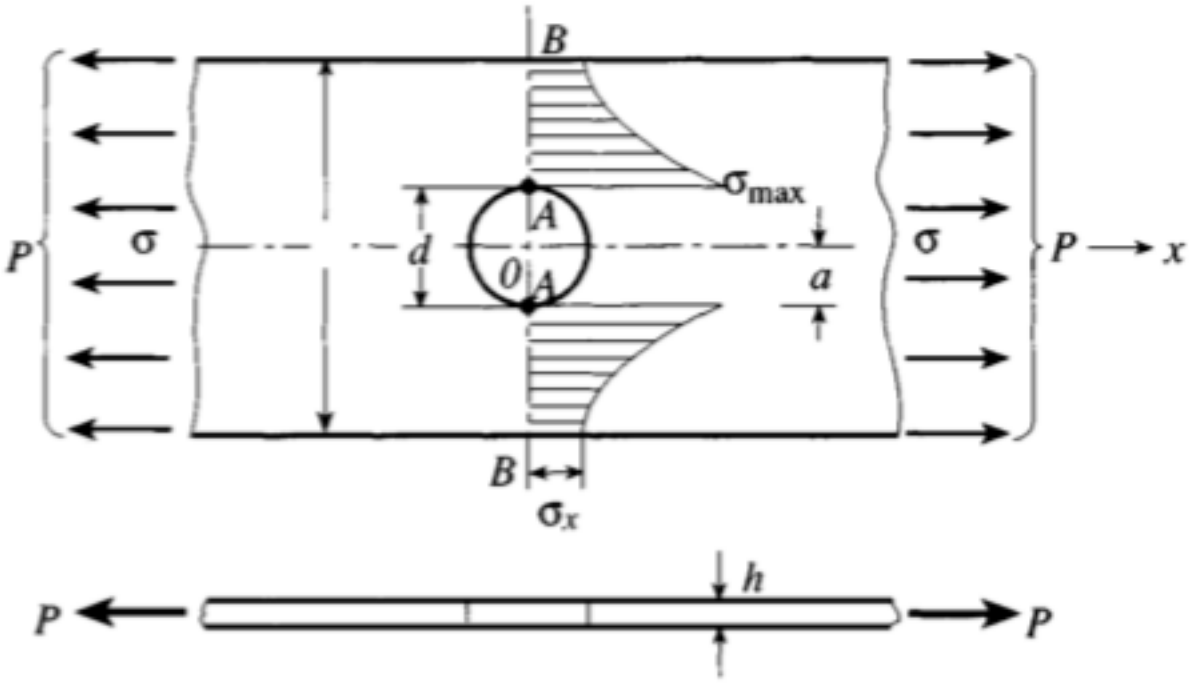

Figure 2.3 Tension bar with a hole [6]

The proper identification of reference stress is necessary for calculation of stress concentration. The reference stress can be given as the ratio of force applied to the gross cross-sectional area. [6]

$$\sigma_{ave} = \frac{P}{Hh} \qquad \text{eqn 2-3}$$

Where,

P is the force applied

H is the width of the sample

h is the thickness

Now, the stress concentration factor becomes

$$K_{tg} = \frac{\sigma_{max}}{\sigma_{ave}} \qquad \text{eqn 2-4}$$

$$K_{tg} = \frac{\sigma_{max}}{\frac{P}{Hh}} = \frac{\sigma_{max}(Hh)}{P} \qquad \text{eqn 2-5}$$

Nominal stress is defined as the force applied to the cross-section area remaining after removing the hole. [6]

$$\sigma_n = \frac{P}{(H-d)h} \qquad \text{eqn 2-6}$$

where, d is the diameter of the hole.

Now, the stress concentration factor for nominal stress becomes

$$K_{tn} = \frac{\sigma_{max}}{\sigma_n} = \frac{\sigma_{max}}{\frac{P}{(H-d)h}} = \frac{\sigma_{max}(H-d)h}{P} = \frac{K_{tg}(H-d)}{H} \qquad \text{eqn 2-7}$$

As we can see the difference in nominal stress, K_{tn} and K_{tg} is distinguish by the ratio of diameter of the hole to the width of the sample (d/H) [6].

2.2.2 Stress concentration at an Elliptical Hole

The solution of Stress concentration for an elliptical hole can be applied to replicate different defects by changing aspect ratio b/a. By letting b$\rightarrow$ 0 the equation can be used for solution of the crack, expressed with the Cartesian coordinates(x,y) [7].

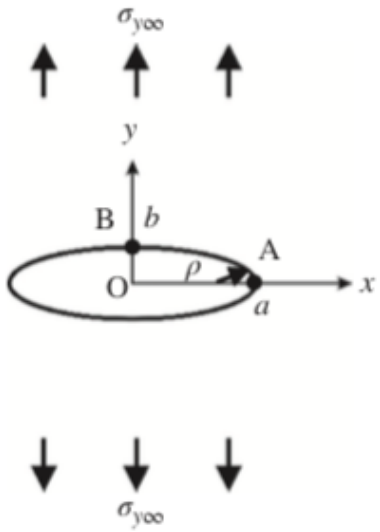

Figure 2.4 Elliptical hole with remote stress [7]

Under remote stress $\sigma_{y\infty}$ or $\sigma_{x\infty}$ the Cartesian coordinates in x-axis can be expressed as,

$$\frac{\sigma_x}{\sigma_{\infty y}} = \left(\frac{1}{(\zeta^2-1)}.\frac{2\lambda+1}{\lambda-1}\right) + \frac{1}{(\zeta^2-1)^2}\left(\frac{1}{2}\left(\frac{a-b}{a+b} - \frac{a+3b}{a-b}\right)\zeta^2 + \frac{(a+b)b}{(a-b)^2}\right) + \frac{4\zeta^2}{(\zeta^2-1)^3}\left(\frac{b}{a+b}\zeta^2 - \frac{b}{a-b}\right)\left(\frac{a}{a-b}\right)$$ *[7]* *eqn 2-8*

For y-axis

$$\frac{\sigma_y}{\sigma_{\infty y}} = \left(\frac{1}{(\zeta^2-1)}.(\zeta^2 + \frac{\lambda}{\lambda-1}\right) - \frac{1}{(\zeta^2-1)^2}\left(\frac{1}{2}\left(\frac{a-b}{a+b} - \frac{a+3b}{a-b}\right)\zeta^2 + \frac{(a+b)b}{(a-b)^2}\right) - \frac{4\zeta^2}{(\zeta^2-1)^3}\left(\frac{b}{a+b}\zeta^2 - \frac{b}{a-b}\right)\left(\frac{a}{a-b}\right)$$ *[7]* *eqn 2-9*

Where, $\lambda = \frac{a}{b}$, $\zeta = \frac{x+(x^2-c^2)^{\frac{1}{2}}}{c}$ c= $\sqrt{a^2-b^2}$

σ_y has the maximum value at point A(x=a). Denoting it by $\sigma_{ymax,}$ we get,

$$\sigma_{ymax} = (1 + (\frac{2a}{b})\sigma_{\infty y}$$

Thus, the stress concentration factor K_t is,

$$K_t = 1 + \frac{2a}{b}$$ *eqn 2-10*

Or, can also be expressed as,

$$K_t = 1 + 2\sqrt{\frac{t}{p}}$$ *eqn 2-11*

Where t=a and p =b^2/a, the radius of the curvature or notch root radius at point A

2.2.3 Finite width effects

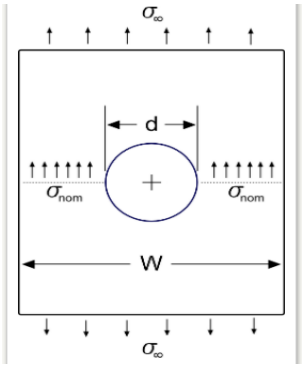

Figure 2.5 finite width effect [8]

There's average stress at the hole due to reduction of cross section area related to uniaxial stress,σ_∞ applied on the finite width plates. The new stress is nominal stress, $\sigma_{nom.}$ The hole on the geometry

decrease the area of the plate and the stress is related to area of the of the body if the force is constant. The stress is more at the edges of the hole. [8]

Here, we know

$$F = \sigma_{\infty} W = \sigma_{nom}(W - d) \quad [8] \qquad \text{eqn 2-12}$$

where,

F is the force.

W is the width.

d is the diameter of hole.

Solving for nominal stress, σ_{nom} we get,

$$\sigma_{nom} = \left(\frac{W}{W-D}\right) \sigma_{\infty} \quad [8] \qquad \text{eqn 2-13}$$

We already have equation for stress concentration factor, K_t which is

$$K_t = \left(\frac{\sigma_{max}}{\sigma_{nom}}\right) \quad [8] \qquad \text{eqn 2-14}$$

For this case σ_{max} is the maximum hoop stress at angle 0 and 180 degree. For the infinite wide plate the ratio of diameter of hole to width of plate is 0, i.e. $\frac{d}{W} \sim 0$. And at this point stress concentration factor, $K_t = 3$. The graph below shows the dependence of K_t to d/W. [8]

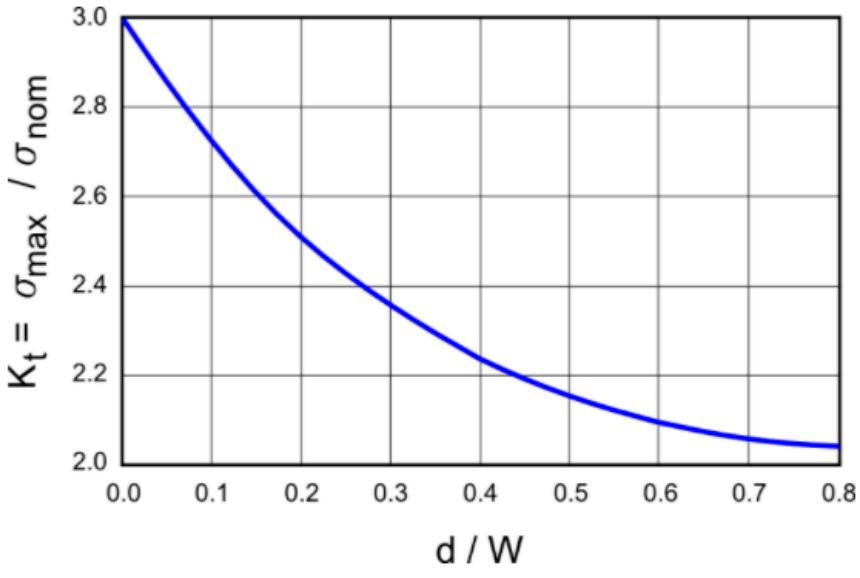

Figure 2.6 graph show relation of stress concentration factor to ratio of diameter of holes to width of plate [8]

Solving the equation of the curve we get,

$$K_t = 3 - 3.14\left(\frac{d}{W}\right) + 3.667\left(\frac{d}{W}\right)^2 - 1.527\left(\frac{d}{W}\right)^3 \quad [8] \qquad \text{eqn 2-15}$$

As it can be seen from the graph that when d/W approach to 1, stress concentration factor decreases to 2.

2.3 Stress concentration for bending flat beam with semicircular notches

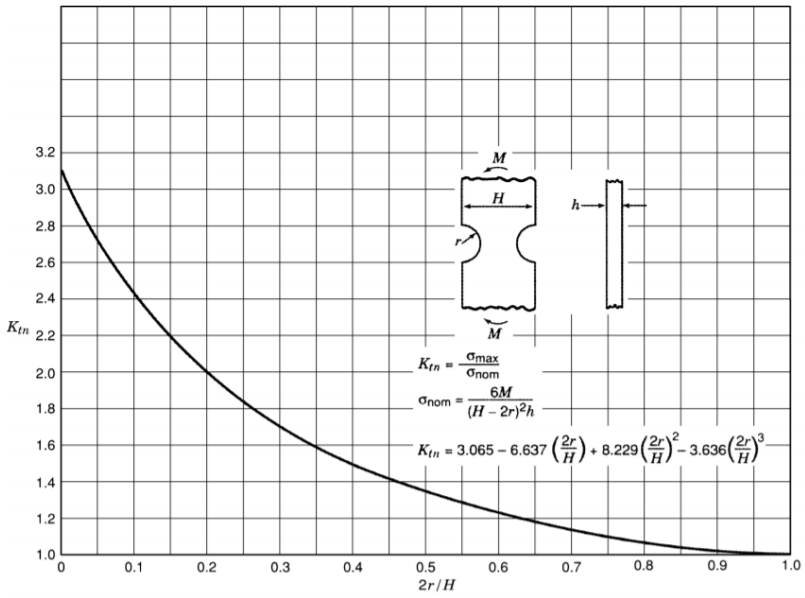

Figure 2.7 Stress concentration factor for bending flat beam with semicircular edge notches [9]

Figure 2.7 shows the stress concentration factor to the nominal stress, K_{tn}, for a flat bending beam with semicircular edges notches with a radius r.

$$K_{tn} = 3.065 - 6.637\left(\frac{2r}{H}\right) + 8.229\left(\frac{2r}{H}\right)^2 - 3.636\left(\frac{2r}{H}\right)^3 \qquad \text{eqn 2-16}$$

where,

K_{tn} is the stress concentration factor

H is the width of the plate

r is the radius of notch

As, it can be seen from the graph that, when 2r/H approach to 1, stress concentration factor decreases to 1.

2.4 Fracture Mechanics

Even a small scratch on the surface can initiates the formation of crack at period of time when stress is applied. Later the crack will propagate and reach at critical point having higher length causing the final fracture of the material. [10]

In high strength materials like composites cracks can change the distribution of local stress in such a way that the elastic stress analysis becomes insufficient. After reaching the critical length, crack can propagate rapidly throughout the specimen causing catastrophic consequences. Fracture mechanics gives the quantitative relation of crack length, its resistance to crack growth and stress where crack grows rapidly. [11]

2.4.1 Fracture Mechanics of Through-Thickness Crack

Griffith had explained the difference between measure and predicted strength of glass considering the stability of small crack using energy balance on the crack. As shown in figure 2.7, the through-thickness crack in a uniaxial stressed plate of infinite width, Griffith considered the strain energy in cracked plate would be less than uncrack plate, finding strain energy released from crack under plane stress conditions with stress analysis given by, [12]

$$U_r = \frac{\pi \sigma^2 a^2 t}{E} \qquad \textit{eqn 2-17}$$

Where,σ = applied stress

U_r= released strain energy,

a =half crack length

t =plate thickness

E =Modulus of Elasticity of the plate

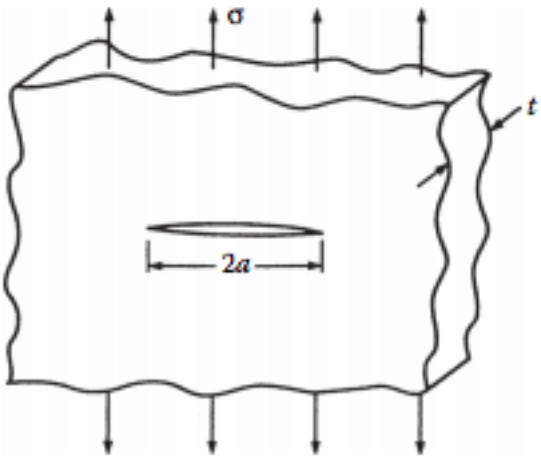

Figure 2.8 Griffith Crack: A through-Thickness crack in a uniaxial stressed plate of infinite width [12]

Here, the Volume of the ellipse $V = 2\pi a^2 t$. So, the strain energy released around the crack due to elliptical relaxation is given by,

$$U_r = \frac{\sigma^2 V}{2E} = \frac{\pi\sigma^2 a^2 t}{E} \qquad \textit{eqn 2-18}$$

According to Griffith assumption, formation of crack requires absorption of energy, U_s Given by [12]

$$U_s = 4at\gamma_s \qquad \textit{eqn 2-19}$$

γ_s, is surface energy per unit area.

As crack grows, the rate of energy absorbed is greater than the rate of stain energy released. Until certain point the crack growth is stable where rate of released energy is greater than absorbed energy. After reaching certain length the growth of crack becomes unstable. When the rate of both absorbed and released energy is equal we get the condition of neutral equilibrium. [12]

$$\frac{\partial U_r}{\partial a} = \frac{\partial U_s}{\partial a} \qquad \textit{eqn 2-20}$$

or, $\frac{\pi\sigma^2 a}{E} = 2\gamma_s$

or, $\sigma\sqrt{\pi a} = \sqrt{2E\gamma_s}$ *eqn 2-21*

When the stress is critical σ_c, we get fracture toughness K_c, given by

$$K_c = \sigma_c\sqrt{\pi a} \qquad \textit{eqn 2-22}$$

2.4.2 Stress Intensity Approach

George R Irwin Develop the concept of Stress Intensity Factor in 1957. According to him, the stress on the crack tip is responsible for rate of crack growth. [13]

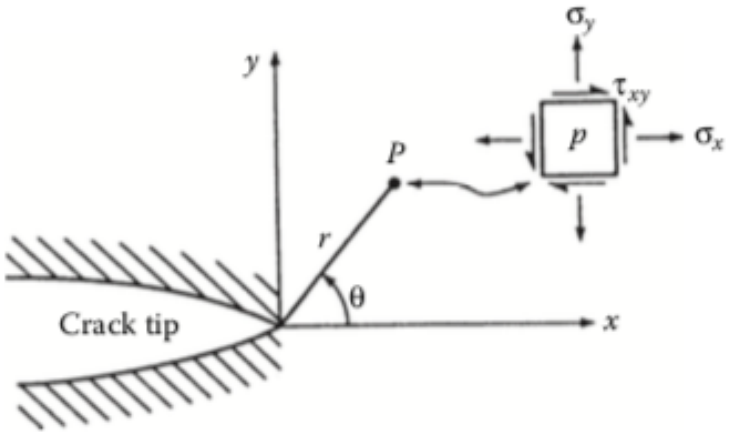

Figure 2.9 Stress at the tip of a crack under plane stress. [12]

Analyzing the stress distribution around the crack tip, the new concept can be developed that can be applied to homogeneous isotropic or anisotropic materials. As represented in figure2-6, using Westergaard solution stress for isotropic case at point P, defined by polar coordinates(r,θ) can be calculated as, [12]

$$\sigma_x = \frac{K_I}{(\sqrt{2\pi r})} cos\left(\frac{\theta}{2}\right)\left(1 - sin\left(\frac{\theta}{2}\right) sin\left(\frac{3\theta}{2}\right)\right) \quad \textit{eqn 2-23}$$

$$\sigma_y = \frac{K_I}{(\sqrt{2\pi r})} cos\left(\frac{\theta}{2}\right)\left(1 + sin\left(\frac{\theta}{2}\right) sin\left(\frac{3\theta}{2}\right)\right) \quad \textit{eqn 2-24}$$

$$\tau_{xy} = \frac{K_I}{(\sqrt{2\pi r})} cos\left(\frac{\theta}{2}\right) sin\left(\frac{\theta}{2}\right) sin\left(\frac{3\theta}{2}\right) \quad \textit{eqn 2-25}$$

Where, K_I is the stress intensity factor for crack opening mode. i.e.

$$K_I = \sigma\sqrt{\pi a} \quad \textit{eqn 2-26}$$

As it's already discussed at critical stress we get fracture toughness, K_c, given as

$$K_c = \sigma_c\sqrt{\pi a}$$

The stress intensity factor differs with the geometry of the crack.

$$K_I = \alpha\sigma\sqrt{\pi a} \qquad \textit{eqn 2-27}$$

Table 2.1 Stress Intensity for different crack types [11]

Types of Crack	Stress Intensity Factor, K_I
Centre crack, length 2a, in an infinite plate	$\sigma_\infty\sqrt{\pi a}$
Edge crack in a semi-infinite plate with crack length a	$1.12\ \sigma_\infty\sqrt{\pi a}$
In an infinite body, central penny shaped crack with radius a	$2\sigma_\infty\sqrt{\frac{a}{\pi}}$
In a plate width W, central crack length 2a	$\sigma_\infty\sqrt{(W\tan(\pi a/W))}$
2 symmetrical edge cracks each length a and in plate total width W	$\sigma_\infty\sqrt{(W(\tan\left(\frac{\pi a}{W}\right)+0.1\sin\left(\frac{2\pi a}{W}\right))}$

Considering the geometry parameter (α)of crack the stress intensity equation becomes,

$$K_I = \alpha\sigma\sqrt{\pi a} \qquad \textit{eqn 2-28}$$

2.5 3-point bending

Flexural modulus, stress-strain behavior and failure limits in bending can be done with 3-point bending test. For the test, surface of the sample is placed in the tension while the outer fibers are subjected to maximum stress and strain. Once the material reaches maximum limits, failure occurs. [14]

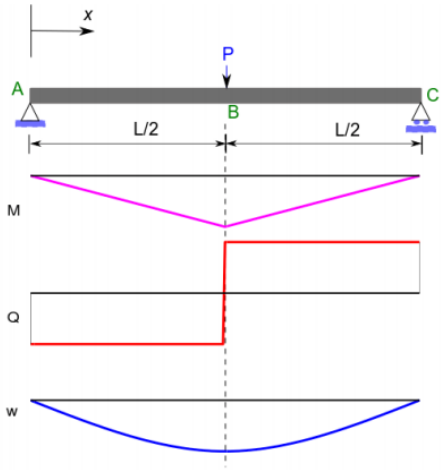

Figure 2.10 Schematic of three-point bend test [15]

Now, the deflection w_o at the center of the beam can be represent as,

$$w_o = \frac{FL^3}{48EI} \qquad \textit{eqn 2-29}$$

Where, E is the bending or flexural modulus and I is the second moment of the area which can be given as,

$$I = \frac{t^3 b}{12} \qquad \textit{eqn 2-30}$$

here, t is the beam's thickness and b is its width.

After calculating deflection w_o, knowing the value of force applied F and measuring the geometry of the sample, flexural modulus can be calculated by using equation

$$E = \left(\frac{FL^3}{48Iw_o}\right) \qquad \textit{eqn 2-31}$$

When the applied force F, is plotted in graph against central displacement w_o, a straight line is obtained whose gradient is, [15]

$$\frac{dF}{dw_o} = \frac{48EI}{L^3}$$ *eqn 2-32*

3 Samples

Two different types of glass fiber laminate composites were manufactured in Arcada's material lab. Then the prepared sheet of samples was water cut into standard size for the analysis. The glass fiber was manufactured and provided by Ahlstrom-Munksjö company located in Helsinki Finland. Two multiaxial glass fibers were used to make two different samples.

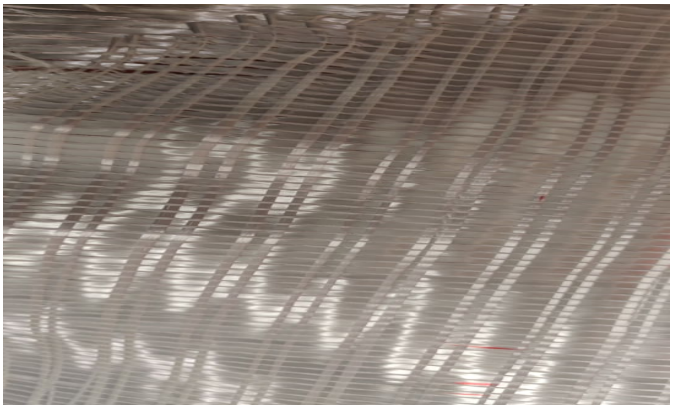

Figure 3.1 Multiaxial glass fibers in direction 0/90/M70

As shown in figure 3-1, textile contain glass fabrics oriented in 0,90 and M70 direction. For easy representation consider the textile as 'A'. From the packaging detail of the product the mass distribution of fabrics in direction 0/90/M70 is 1152/51/70 g/m^2. So, total mass distribution is found to be 1,273 g/m^2.

Figure 3.2 Details of textile 'A' provided by company on packaging

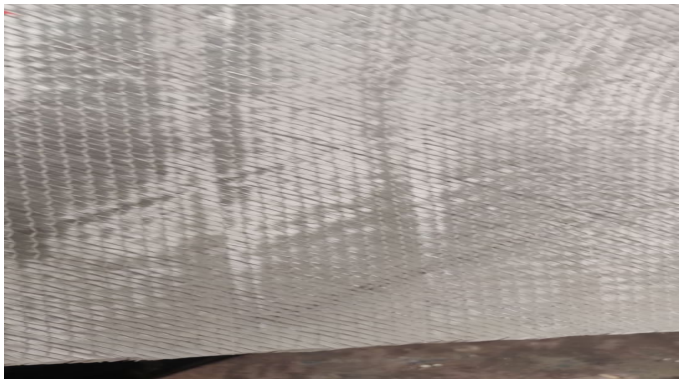

Figure 3.3 Multiaxial glass fiber in direction +45/-45/ M100

In figure 3-3, textile contain glass fabrics oriented in +45, -45 and M100 direction. For easy representation consider the textile as 'B'. From the packaging detail of the product the total mass distribution of fabrics is 723 g/m^2 where 311.5 g/m^2 is distributed in each direction +45/-45 and 100g/m^2 in M100.

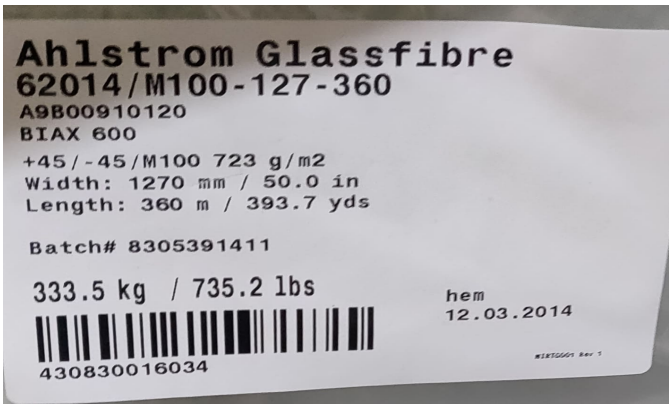

Figure 3.4 Details of textile 'B' provided by company on packaging

3.1 ABA symmetrical

The laminate composite is prepared with six layers of textile where the fabrics are oriented in direction A (0, 90, M70) B (+45, -45, M100) A (0, 90, M100) symmetrically. The sheet prepared then is water cut into the suitable size that can be used for testing and analyzing. The total fiber mass distribution is found to be 6,538 g/m^2.

Figure 3.5 ABA symmetrical samples

The sample ABA9 is thrown away, as the certain area of the sample is delaminated. The measurements of the samples were taken. The ABD matrix calculator is used to find the various factors including fiber volume fraction(f), thickness of sample((t) mm), Width((W) mm), total mass((M)g), total density((D)kg/m^3), fiber density(kg/$m^{3)}$, resin density(kg/$m^{3)}$, fiber mass(kg/m^2) E1(GPa), E2(GPa), G12(GPa), v12.

Table 3.1 Excel table with physical and mechanical measurements of ABA symmetrical sample

Samples	W(mm)	t (mm)	M(g)	f	D		E1	E2	G12	v12
ABA 1	15.20	5.30	25.99	0.49	1825.07		36.34	7.43	2.76	0.30
ABA 2	15.20	5.40	25.89	0.48	1812.57		35.68	7.31	2.72	0.30
ABA 3	15.10	5.40	25.54	0.48	1812.57	Fiber density	35.68	7.31	2.72	0.30
ABA 4	15.20	5.50	26.43	0.47	1800.52	2540.00	35.02	7.18	2.67	0.30
ABA 5	15.20	5.30	26.15	0.49	1825.07	resin density	36.34	7.43	2.76	0.30
ABA 6	15.20	5.35	26.03	0.48	1818.76	1150.00	35.68	7.31	2.72	0.30
ABA7	15.20	5.30	26.02	0.49	1825.07	Fiber Mass	36.34	7.43	2.76	0.30
ABA 8	15.20	5.40	26.80	0.48	1812.57	6.54	35.68	7.31	2.72	0.30
ABA 10	15.20	5.40	26.61	0.48	1812.57		35.68	7.31	2.72	0.30
ABA 11	15.15	5.40	25.93	0.48	1812.57		35.68	7.31	2.72	0.30
ABA 12	15.20	5.45	26.31	0.47	1806.49		35.02	7.18	2.67	0.30
ABA 13	15.20	5.50	26.20	0.47	1800.52		35.02	7.18	2.67	0.30
ABA 14	15.25	5.60	26.18	0.46	1788.91		34.36	7.06	2.63	0.30
ABA 15	15.15	5.25	25.58	0.49	1831.50		36.34	7.43	2.76	0.30
ABA 16	15.20	5.50	26.68	0.47	1800.52		35.02	7.18	2.67	0.30

3.2 BAB symmetrical

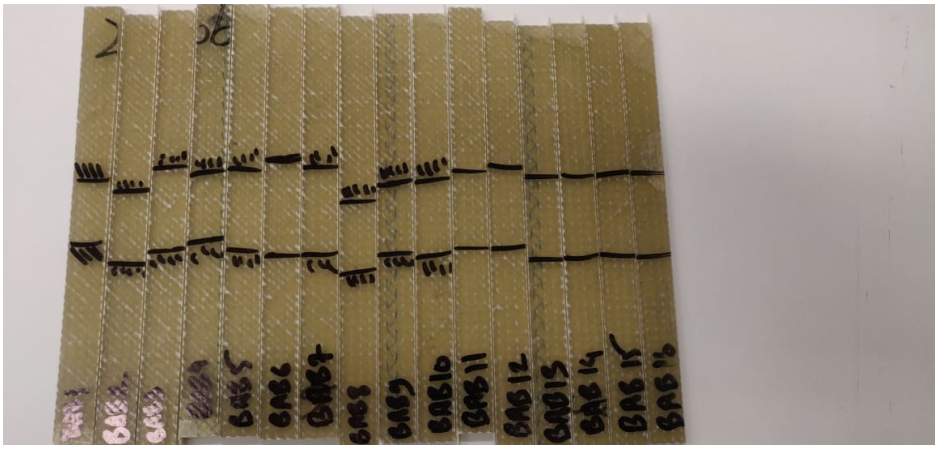

Figure 3.6 BAB symmetrical samples

As like previous sample, these samples also contain six layers of textile where fabrics are oriented in direction B (+45, -45, M100) A (0, 90, M70) B (+45, -45, M100) symmetrically. The total fiber mass distribution is found to be 5,438 g/m^2. The sample BAB16 is thrown away as it also has delaminated area.

Table 3.2 Excel table with physical and mechanical measurements of BAB symmetrical samples

Samples	W(mm)	t(mm)	M(g)	f	D		E1	E2	G12	v12
BAB 1	15.00	4.10	20.12	0.52	1875.83		38.32	7.85	2.92	0.30
BAB 2	15.05	4.05	20.34	0.53	1884.79		38.98	8.00	2.97	0.30
BAB 3	15.05	4.15	20.10	0.52	1867.09	Resin Density	38.32	7.85	2.92	0.30
BAB 4	15.00	4.15	20.23	0.52	1867.09	1150.00	38.32	7.85	2.92	0.30
BAB 5	15.10	4.00	20.28	0.54	1893.98	fiber mass	39.64	8.15	3.03	0.30
BAB 6	15.00	4.15	20.31	0.52	1867.09	5.44	38.32	7.85	2.92	0.30
BAB 7	15.15	4.30	20.52	0.50	1842.07	Fiber Density	37.00	7.57	2.81	0.30
BAB 8	15.10	4.10	20.57	0.52	1875.83	2540.00	38.32	7.85	2.92	0.30
BAB 9	15.00	4.10	20.65	0.52	1875.83		38.32	7.85	2.92	0.30
BAB 10	15.10	4.35	20.39	0.49	1834.12		36.34	7.43	2.76	0.30
BAB 11	15.10	4.15	20.41	0.52	1867.09		38.32	7.85	2.92	0.30
BAB 12	15.20	4.25	20.62	0.50	1850.21		37.00	7.57	2.81	0.30
BAB 13	15.00	4.15	20.53	0.52	1867.09		38.32	7.85	2.92	0.30
BAB 14	15.10	4.20	20.65	0.51	1858.55		37.66	7.71	2.87	0.30
BAB 15	15.15	4.00	20.29	0.54	1893.98		39.64	8.15	3.03	0.30

4 Microscope Analysis

The surface of samples was studied under the microscope, Olympus 800. Before analyzing sample under the microscope, the peel ply was removed and the surface of the all samples were polished. was analyzed under the microscope. The suitable magnification was used under reflection mode to analyzed the defects. Though, mainly 10x magnification was used and on few cases 4x as well. Images were then taken at same resolution 1280x1024, for each defect seen on the surface. Those defects were counted and looked at their geometry and dimension. The measurement of the defects was done using the reference plate which has 10 microns for each division.

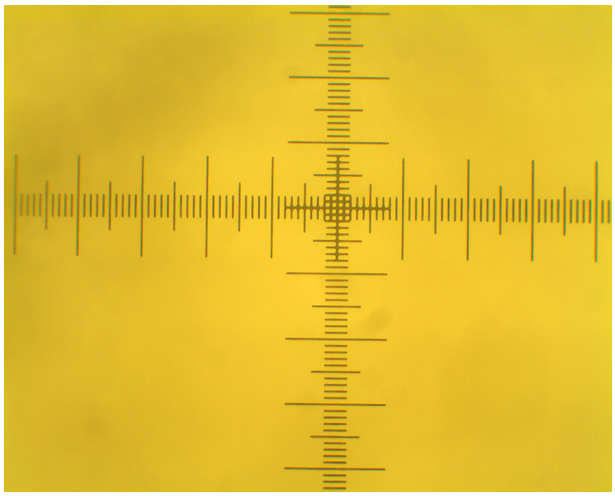

Figure 4.1 Reference plate at 10x magnification

4.1 Defects

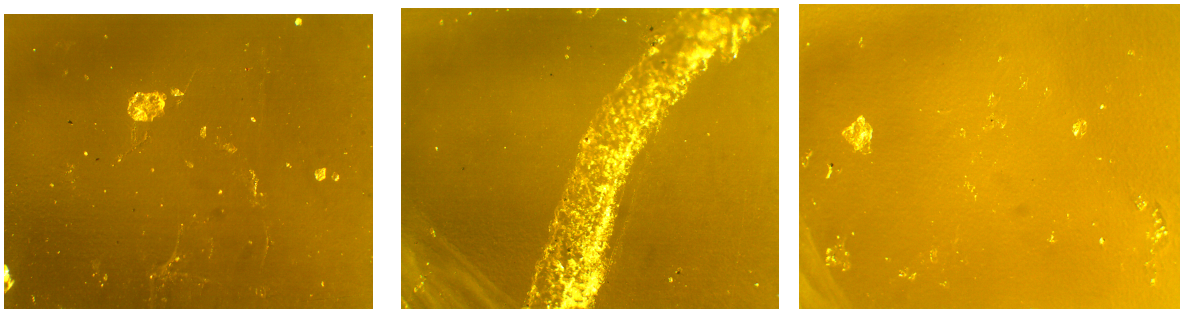

Figure 4.2 Defects on some samples ABA under magnification 10X

Figure 4.2 shows some of the defects detected in samples ABA under 10X magnification. At the top right corner and left corner images, we can see some small air bubbles and voids. The image on the middle is a long circular hole which was formed due to the pull out of the fiber. These kinds of defects were seen on other ABA samples expect on ABA16.

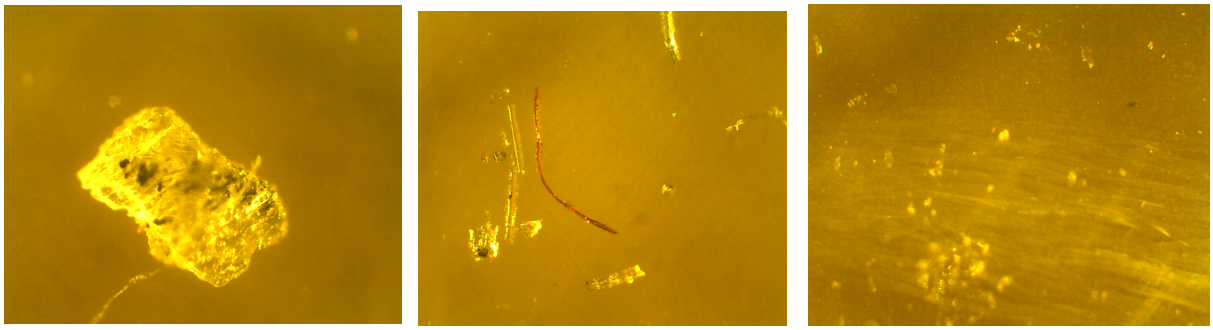

Figure 4.3 Defects on some samples BAB under magnification 10X

Figure 4.3 shows some of the defects seen on the sample BAB under magnification of 10X. At the top left image, we can see a void in the surface of the sample. At top left image, we can see small dot like geometry which are air bubbles on the surface. As the air bubbles are in different depth of the surface the focus on defects is not clear on the image. On image in the center, we can see a red thread like structure which is not supposed to be there. This could be the impurity in the fibers. Also, some voids and air bubbles can be seen on the same image. These kinds of defects were seen on other BAB samples as well except for BAB8, BAB10 and BAB11.

The defects detected from the microscope analysis was then quantified and the dimension was measured using the reference plate. The voids and air bubbles were assumed to be circular hole. The tables below show the number of defects detected in the samples with their diameter.

Table 4.1 Defects on sample ABA with their dimension

Samples	num of defects	defects daimeter(10^1 microns)
ABA 1	1	6
ABA 2	7	2,1,1,1,4,3,1
ABA 3	7	2,2,2,2,2,2,2
ABA 4	4	7, 3 ,4 ,5
ABA 5	3	10,5,7
ABA 6	8	5,1,2,3,1,7,2,2
ABA7	4	3,2,1,1
ABA 8	6	5,3,2,4,1,1
ABA 10	2	1,2
ABA 11	3	1,1,1
ABA 12	3	2,2,1
ABA 13	8	10,3,1,1,3,1,1,1
ABA 14	7	1,1,1,1,1,1,1
ABA 15	3	2,1,1
ABA 16	0	0

Table 4.1 shows the defects detected from microscope analysis of ABA samples. As it can be seen from the table that, the sample ABA13 and ABA6 has highest number of defects (8) detected. On ABA1 only 1 defect in the surface was detected whereas on ABA16 no defects were detected. The smallest defect detected were of 10 microns whereas the biggest was of 100 microns.

Table 4.2 Defects on sample BAB with their dimension

Samples	No. of defects	defect's diameter(10^1micron)
BAB1	3	2, 1 ,1
BAB2	2	2,2
BAB3	8	6,8,9,4,3,8,9,10
BAB4	8	7,5,1,3,2,5,4,2
BAB5	3	5,1,1
BAB6	4	5,3,3,1
BAB7	5	5,1,2,2,3
BAB8	0	0
BAB9	3	2,2,1
BAB10	0	
BAB11	0	
BAB12	1	10
BAB13	2	1, 1
BAB14	3	3 ,3 ,2
BAB15	2	6 ,2

Table 4.2 shows the defects detected from microscope analysis of BAB samples. As it can be seen from the table that, the sample BAB3 and BAB4 has highest number of defects (8) detected. On BAB12 only 1 defect in the surface was detected whereas on BAB8, BAB10, BAB11 no defects were detected. The smallest defects detected were of 10 microns whereas the biggest was of 100 microns.

5 Stress concentration factor

After analyzing specimens, the defects on the surface are detected. Mostly air bubbles and voids are seen on samples. Considering air bubbles and voids as semicircular notch edges on the plate under bending load, the stress concentration factor for defects was calculated and expressed as,

$$K_t = 3.065 - 6.37\left(\frac{2r}{W}\right) + 8.229\left(\frac{2r}{W}\right)^2 - 3.636\left(\frac{2r}{W}\right)^3 \qquad \textit{eqn 5-1}$$

where 'r' is the radius of the defects and 'W' is the width of the sample,

Table 5.1 Stress concentration on defects of samples BAB

Samples	Width(mm)	No. of defects	defect's diameter(10^1micron	Stress Concentration fcator (Kt)
BAB1	15	3	2, 1 ,1	3,3,3
BAB2	15.02	2	2,2	3,3
BAB3	15.05	8	6,8,9,4,3,8,9,10	3,3,3,3,3,3,3,3
BAB4	15	8	7,5,1,3,2,5,4,2	3,3,3,3,3,3,3,3
BAB5	15.1	3	5,1,1	3,3,3
BAB6	15	4	5,3,3,1	3,3,3,3
BAB7	15.15	5	5,1,2,2,3	3,3,3,3,3
BAB8	15.1	0	0	0
BAB9	15	3	2,2,1	3,3,3
BAB10	15.1	0		0
BAB11	15.1	0		0
BAB12	15.2	1	10	3
BAB13	15	2	1, 1	3,3
BAB14	15.1	3	3 ,3 ,2	3,3,3
BAB15	15.15	2	6 ,2	3,3

Table 5.2 Stress Concentration on defects of sample ABA

Samples	Width(mm)	No. of defects	defect's diameter(10^1 micron)	Stress Concentration factor(Kt)
ABA1	15.2	1	6	3
ABA2	15.2	7	2,1,1,1,4,3,1	3,3,3,3,3,3,3
ABA3	15.1	7	2,2,2,2,2,2,2	3,3,3,3,3,3,3
ABA4	15.2	4	7, 3 ,4 ,5	3,3,3,3
ABA5	15.2	3	10,5,7	3,3,3
ABA6	15.2	8	5,1,2,3,1,7,2,2	3,3,3,3,3,3,3,3
ABA7	15.2	4	3,2,1,1	3,3,3,3
ABA8	15.2	6	5,3,2,4,1,1	3,3,3,3,3,3
ABA10	15.2	2	1,2	3,3
ABA11	15.15	3	1,1,1	3,3,3
ABA12	15.2	3	2,2,1	3,3,3
ABA13	15.2	8	10,3,1,1,3,1,1,1	3,3,3,3,3,3,3,3
ABA14	15.25	7	1,1,1,1,1,1,1	3,3,3,3,3,3,3
ABA15	15.15	3	2,1,1	3,3,3
ABA16	15.2	0	0	0

Table 5.1 and Table 5.2 shows the stress concentration on BAB and ABA samples respectively. The samples possessed number of air bubbles on the analyzed surface. On some samples like ABA16, BAB8, BAB10, BAB11 no air bubbles were detected from the magnification used from microscope

analysis so no calculation was done for them. Depending upon the number of defects in the samples, stress is concentrated on different number of places. As it seen from the calculation that the stress concentration on all the defects detected is found to be 3. Stress Concentration factor is calculated in relation with ratio of defects diameter to width of the sample and the defects appeared on the samples are significantly lower to comparison with the width.

6 3-point Bending Test

Universal Testing Machine was used for three-point bending test of the samples. Force was applied on the sample resting on the beam of testing machine at a distance of 100 mm as shown in figure below,

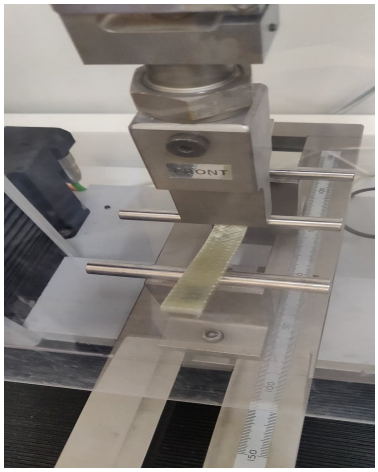

Figure 6.1 3-point bending test of sample

The sample starts to bend after the force is applied. It reaches to certain deflection and I could hear the cracking sound of the ply. The force is applied on the sample until the certain bending length. Some samples broke completely at the bending length but some samples did not break at the bending length. After that data can be obtained from the experiment which shows the relation between Force applied to the deflection on the sample, x.

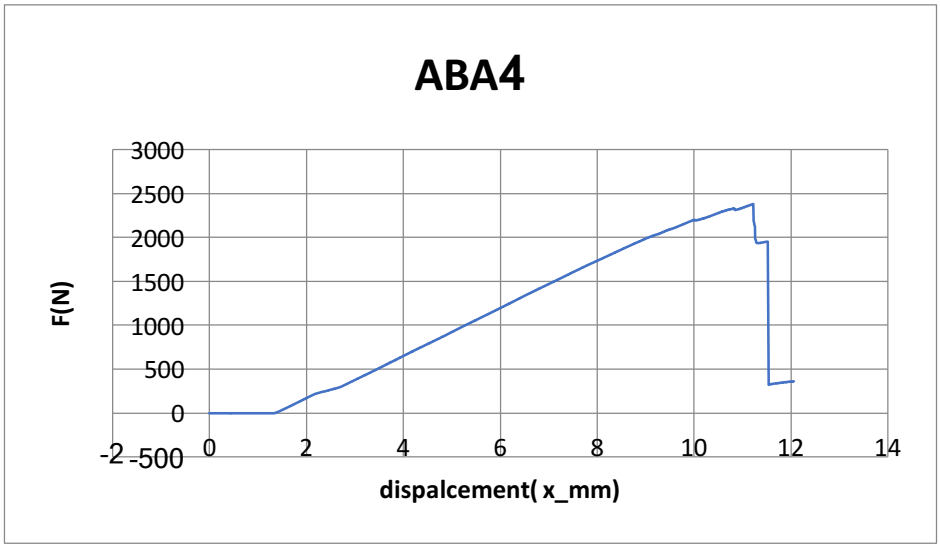

Figure 6.2 Graphical relation of Force applied to deflection on sample ABA4

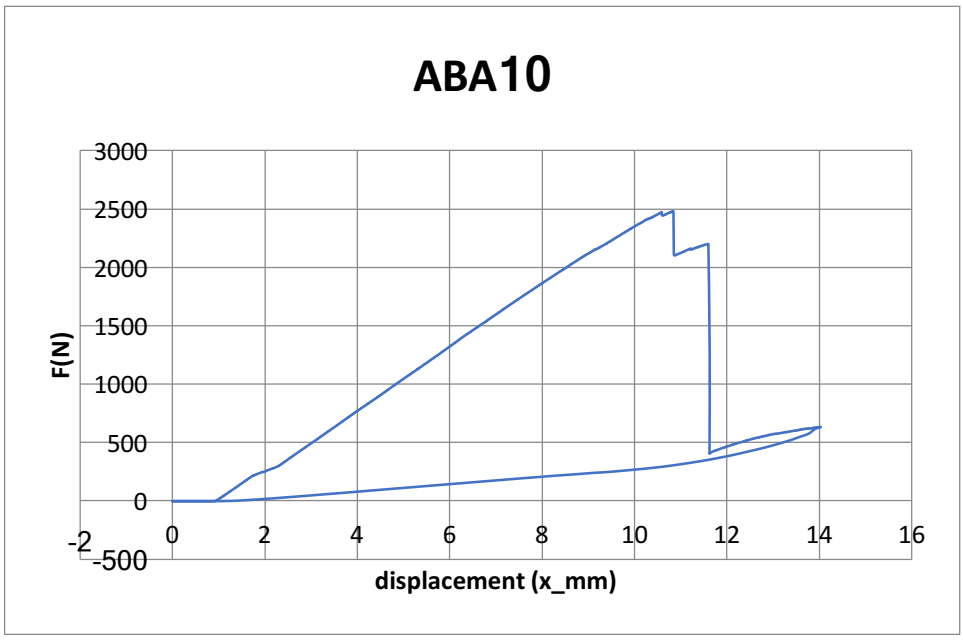

Figure 6.3 Graphical relation of Force applied to deflection on sample ABA10

Above graphs show the relation between force and deflection on few of the samples used. The graph shows information about mechanical failure of the sample. As seen on the graphs, as force increased the deflection on the sample increase.

For ABA4 and ABA10 samples, the graph shows that it will start breaking at some point but still it does not fail completely. After that point, the samples slowly break but can still withstand certain force for a while but after certain point the sample fails completely. Graphs in figure 6-3 and 6-4,

we can see certain deflection on the curve which is the point where the sample just start to break it means there's breakage on certain ply of the composites. The force applied decrease at the point but the curve goes slowly up which means the sample is still withstanding force and is not failed completely. At some point the curve goes down suddenly and the curve does not go up, it's the point where the sample is completely failed.

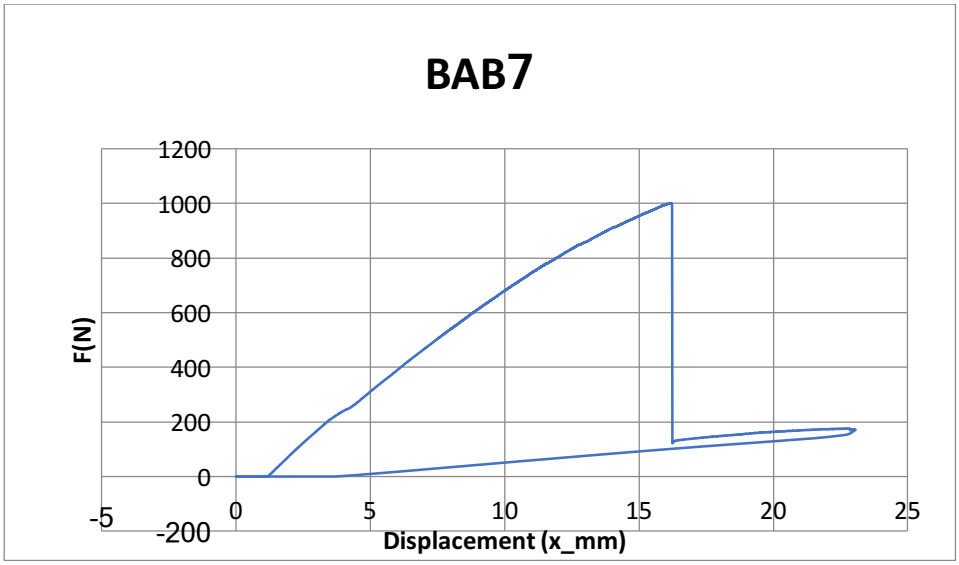

Figure 6.4 Graphical relation of Force applied to deflection on sample BAB7

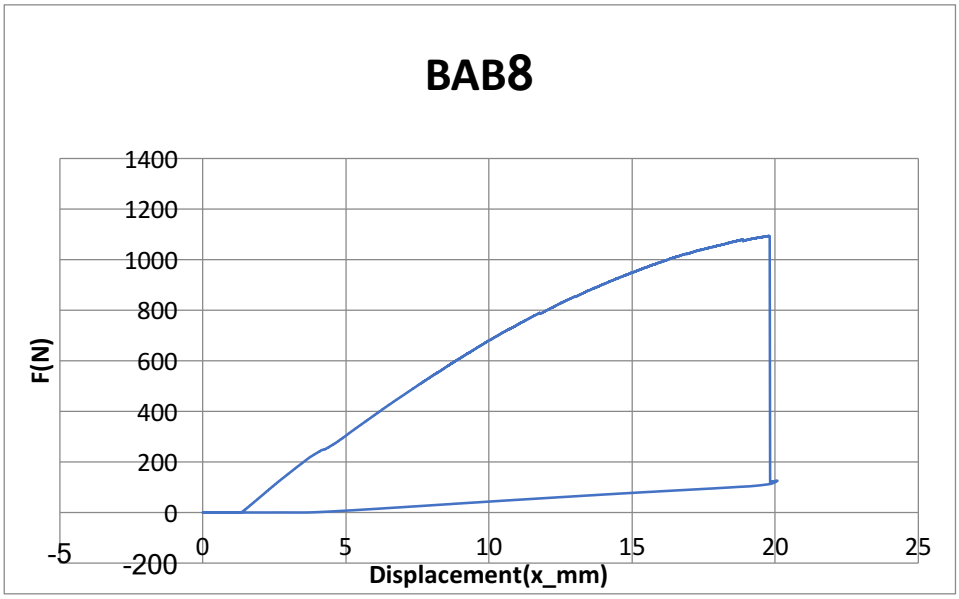

Figure 6.5 Graphical relation of Force applied to deflection on sample BAB8

Figure 6.4 shows the brittle failure of sample BAB7. It can be seen on the figure 6-4 the force is applied on sample BAB7, as the force increase the displacement on the specimen increase. When the force reached the value of 998.60 N the sample was displaced 16.22mm downward at which point the sample could not withstand more force as a result of which it breaks suddenly. The sample continued to bend further but there was very less resistance force. But in case of sample BAB8, from figure 6.5 it can be seen that the sample did not fail completely, rather it went through partial plastic deformation.

The graphs for the samples were obtained such as above depending upon whether the sample broke completely or not. The data obtained from the graph is now used to find the stress failure and strain failure of samples. eqn 2-27, eqn 2-28 and eqn 2-29 are used to find the value of second moment of area I, flexural modulus E where L is the distance between the beam on testing machine.

Table 6.1 Mechanical properties with Stress and Strain Failure of BAB samples

Samples	F_max(N)	x(mm)	slope(N/mm)	L(mm)	W(mm	t (mm)	I [mm^4]	E(Mpa)	Strain_failure	Stress_failure[Mpa]
BAB1	1043.10	20.67	90.77	100.00	15.00	4.10	86.15	21950.25	0.05	620.52
BAB2	1059.08	20.11	83.37	100.00	15.05	4.05	83.31	20847.22	0.05	643.54
BAB3	956.40	18.48	85.42	100.00	15.05	4.15	89.64	19853.36	0.05	553.48
BAB4	1033.80	21.11	86.67	100.00	15.00	4.15	89.34	20209.39	0.05	600.26
BAB5	1012.60	20.10	88.80	100.00	15.10	4.00	80.53	22971.34	0.05	628.68
BAB6	1108.60	22.47	93.18	100.00	15.00	4.15	89.34	21729.30	0.06	643.69
BAB7	998.60	16.22	95.61	100.00	15.15	4.30	100.38	19844.03	0.04	534.73
BAB8	1090.90	19.81	94.86	100.00	15.10	4.10	86.73	22788.35	0.05	644.66
BAB9	1156.30	22.52	92.47	100.00	15.00	4.10	86.15	22361.59	0.06	687.86
BAB10	1110.00	21.16	95.19	100.00	15.10	4.35	103.58	19145.77	0.06	582.72
BAB11	1087.90	20.42	90.46	100.00	15.10	4.15	89.94	20954.87	0.05	627.49
BAB12	1017.50	17.35	95.33	100.00	15.20	4.25	97.24	20425.72	0.04	555.91
BAB13	1079.70	21.14	91.61	100.00	15.00	4.15	89.34	21361.33	0.05	626.91
BAB14	1107.30	20.91	95.06	100.00	15.10	4.20	93.23	21243.08	0.05	623.56
BAB15	891.40	17.63	88.90	100.00	15.15	4.00	80.80	22921.82	0.04	551.61

The table 6.1 shows the data obtained by calculating the experimental data obtained from 3-point bending test of sample BAB symmetrical. The data shows the maximum force applied on the samples. As an instant, for sample BAB1 the maximum force applied on the sample was 1043.10 which displaced the body placed under the force to 20.67mm downwards. Flexural modulus was found to be 21950.25 MPa. The value for stress failure and strain failure was measured to be 620.52 MPa and 0.05 respectively which means that the sample fails at the given value of stress and strain.

Table 6.2 Mechanical properties with Stress and strain failure of ABA samples

Samples	F_max(N)	x(mm)	slope(N/mm)	L(mm)	W(mm)	t(mm)	I[mm^4]	E(Mpa)	Strain_failure	Stress_failure[Mpa]
ABA1	2371.40	10.14	261.79	100.00	15.20	5.30	188.58	28921.57	0.03	833.11
ABA2	1927.40	9.00	238.05	100.00	15.20	5.40	199.45	24864.71	0.03	652.28
ABA3	1983.30	11.20	230.17	100.00	15.10	5.40	198.14	24200.84	0.04	675.64
ABA4	2283.50	11.23	269.13	100.00	15.20	5.50	210.74	26605.44	0.04	744.94
ABA5	2197.00	11.82	252.91	100.00	15.20	5.30	188.58	27940.54	0.04	771.84
ABA6	2354.00	11.50	211.40	100.00	15.20	5.35	193.97	22705.97	0.04	811.61
ABA7	2299.70	11.03	253.52	100.00	15.20	5.30	188.58	28007.93	0.04	807.92
ABA8	2291.70	9.83	236.00	100.00	15.20	5.40	199.45	24650.58	0.03	775.56
ABA10	2464.30	10.55	268.90	100.00	15.20	5.40	199.45	28087.04	0.03	833.98
ABA11	2296.90	11.60	247.57	100.00	15.15	5.40	198.80	25944.43	0.04	779.89
ABA12	2151.20	9.68	225.16	100.00	15.20	5.45	205.05	22876.95	0.03	714.72
ABA13	2147.60	9.67	229.00	100.00	15.20	5.50	210.74	22638.30	0.03	700.61
ABA14	2538.90	10.80	252.48	100.00	15.25	5.60	223.18	23568.56	0.04	796.33
ABA15	2027.40	9.73	230.96	100.00	15.15	5.25	182.69	26338.21	0.03	728.28
ABA16	2321.70	9.90	226.02	100.00	15.20	5.20	178.10	26438.28	0.03	847.32

Table 6.2 shows the experimental data obtained from data from 3-point bending test of ABA symmetrical samples. The table shows the strain and stress failure of the samples on the maximum force applied. For example, for sample ABA1 the specimen deflects to 10.14mm with a force of 2371.10 N which is the failure point of a sample. The sample fails at the strain value of 0.03 and stress failure at 833.11 MPa. The experimental flexural modulus of the sample is found to be 28921.57 MPa.

7 Theoretical Calculation

Composite Compressive Strength Modeller(CCSM) calculator was used to calculate the theoretical stiffness of the samples. The calculation was done considering the sample without any defects. Each sample were made by symmetrical arrangement of two fabrics sheet given name by 'A' and 'B'. And each fabric sheet has three plies oriented in different direction. For fabric sheet A, there were three plies which were in direction of 0 and 90-degree angle, the third ply was m70 which was supposed to be at 0-degree angle for calculation. The mass distribution for 0,90 and m70 plies was 1152 g/m^2, 51 g/m^2 and 70 g/m^2 respectively. For fabric sheet B, the plies were in the direction of +45, -45-degree angle and the third ply was m100 which was supposed to be 0-degree angle for calculation. Compiling six fiber sheets for ABA and BAB symmetrical samples we obtained the specimens with 18 plies of fiber orientation. The plies have different thickness which was calculated from ABD matrix calculator. And the data obtain from ABD matrix thickness(t), E11, E22, G12 and Nu12 for each ply were input on the CCSM calculator.

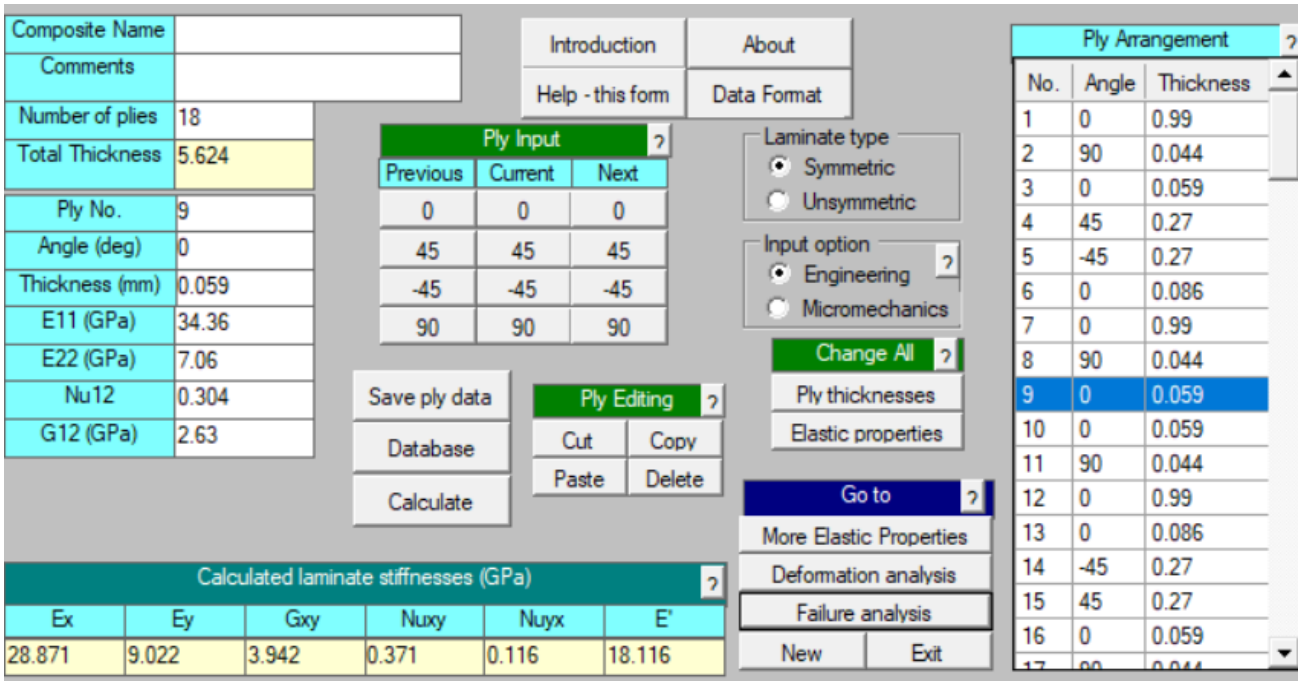

Figure 7.1 Example of Calculation on CCSM calculator

After data were input of all plies, the calculation for laminate stiffness was done. Calculation gave us the value of flexural modulus, Young's modulus normal to fibers E_y, Shear Modulus G_{xy}, and Poisson's ratio Nuxy and bending Modulus E^1. The values are in unit GPa.

After the calculation of laminate stiffness, the failure analysis was done. The database of material E-glass/470-36 was chosen for analysis. The material used in my samples has the similar database to E-glass/470-36.

Material Name	Longitudinal tensile strength SL+	Longitudinal compressive strength SL-	Transverse tensile strength ST+	Transverse compressive strength ST-	In-plane shear strength SLT
AS/3501	1448	1172	48.3	248	62.1
Kevlar 49/epoxy	1379	276	27.6	64.8	60
Scotchply 1002	1103	621	27.6	138	82.7
E-glass/470-36	584	803	43	187	64

Figure 7.2 Database selection for failure analysis.

The failure criterion was done under maximum stress. As bending test was done for experimental failure analysis where the sample was bended downwards. So, for theoretical failure analysis force pattern applied to laminate was all kept value zero expect for Mx(MN). This implies that the load is

applied on the body and bending moment of the body is in x direction downward. The value for Mx is kept being 1 MN. The completion of calculation gives the idea about the ply which was supposed to fail first and the force to give failure.

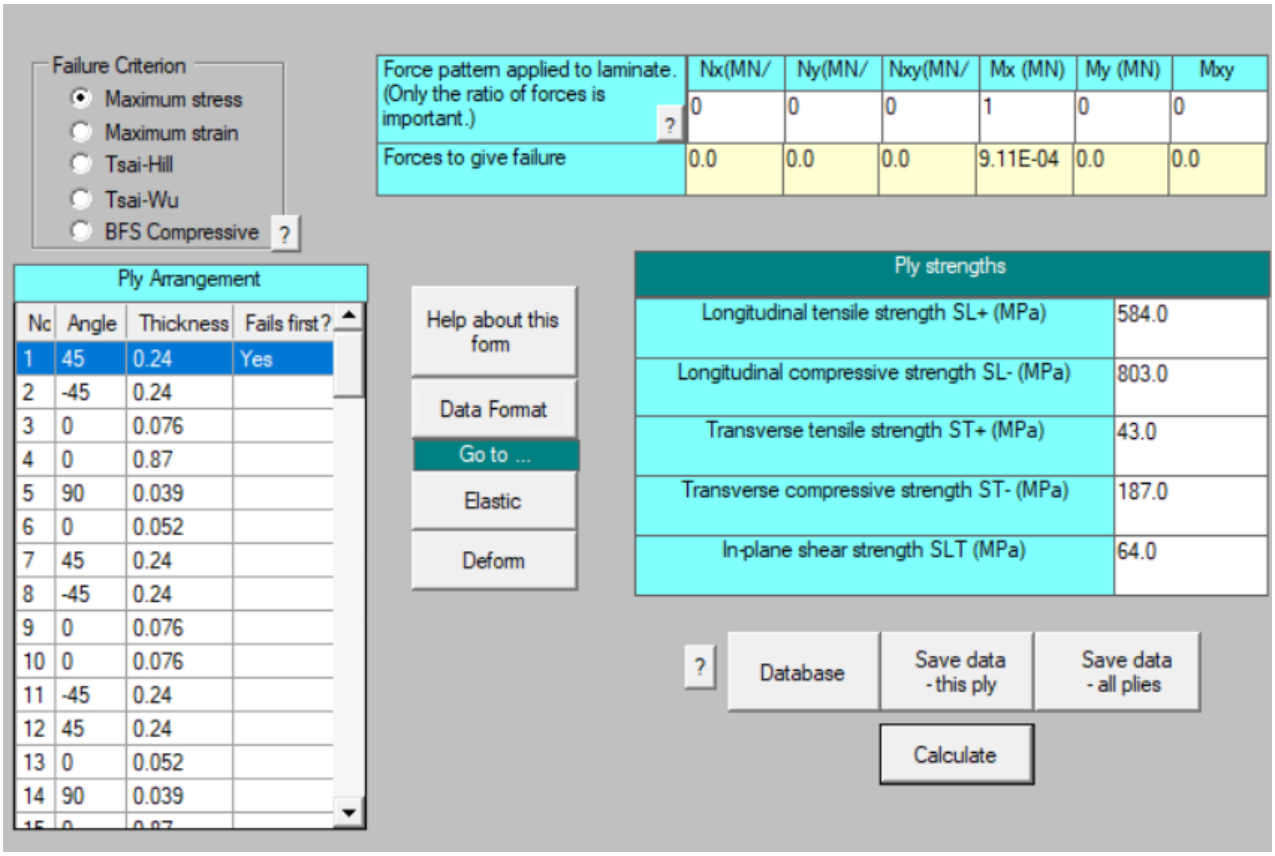

Figure 7.3 Failure analysis of a sample on CCSM calculator

Figure7.3 shows the CCSM calculation window for failure analysis of a sample in failure criterion of maximum stress. The table on top right window shows the value of force applied and the force to give failure to the laminate. Table titled ply strengths shows the database of E-glass/470-36 material use as reference. The table on left side of window shows the ply arrangement and where the ply is supposed to fail first. In this case ply number 1 fails first.

The data obtained from the CCSM calculator for all the samples are given below in the table, where f is the fiber volume fraction, Flexural modulus E_x (GPa), Young's modulus normal to fibers E_y(GPa), Shear Modulus G_{xy}(GPa), and Poisson's ratio Nuxy , the ply supposed fail first, bending moment per unit of width of laminate plate along x direction MX(MN), force to give failure F(f)MN.

Table 7.1 CCSM Calculation for ABA samples

Samples	f	Ex	Ey	Gxy	Nuxy	Nuyx	E'	Ply failure	MX	F(f)MN
ABA 1	0.49	30.605	9.477	4.14	0.37	0.115	19.12	17	1	0.001
ABA 2	0.48	29.971	9.339	4.089	0.371	0.116	18.79	17	1	0.002
ABA 3	0.48	29.971	9.339	4.089	0.371	0.116	18.79	17	1	0.002
ABA 4	0.47	29.313	9.221	4.034	0.372	0.117	18.46	17	1	0.002
ABA 5	0.49	30.605	9.477	4.14	0.37	0.115	19.12	17	1	0.001
ABA 6	0.48	29.971	9.339	4.089	0.371	0.116	18.79	17	1	0.002
ABA7	0.49	30.605	9.477	4.14	0.37	0.115	19.12	17	1	0.001
ABA 8	0.48	29.971	9.339	4.089	0.371	0.116	18.79	17	1	0.002
ABA 10	0.48	29.971	9.339	4.089	0.371	0.116	18.79	17	1	0.002
ABA 11	0.48	29.971	9.339	4.089	0.371	0.116	18.79	17	1	0.002
ABA 12	0.47	29.313	9.221	4.034	0.372	0.117	18.46	17	1	0.001
ABA 13	0.47	29.313	9.221	4.034	0.372	0.117	18.46	17	1	0.001
ABA 14	0.46	28.919	9.008	3.926	0.371	0.115	18.1	17	1	0.002
ABA 15	0.49	30.605	9.477	4.14	0.37	0.115	19.12	17	1	0.001
ABA 16	0.47	29.313	9.221	4.034	0.372	0.117	18.46	17	1	0.001

Table 7.1 shows the data obtained from CCSM calculation of samples ABA symmetric. For sample ABA1 with fiber volume fraction of 0.49 the flexural modulus is found to 30.605 GPa. And when 1 mega newton force is applied to a bending moment of per unit length width of sample ply 17 fails first where 0.001 MN force gives the failure. Comparing the flexural modulus of the sample from Table7.1 i.e. 30.605 GPa to that of Table 6.2 which is 28.921 GPa, we can see that there's decrease on the experimental strength of the sample. Same case applies for all ABA symmetric samples.

Table 7.2 CCSM calculation of BAB samples

Samples	f	Ex	Ey	Gxy	Nuxy	Nuyx	E'	ply failue	MX	F(f)MN
BAB 1	0.52	25.15	10.926	6.379	0.418	0.209	20.509	1, 18	1	0.0009
BAB 2	0.53	25.47	11.128	6.523	0.482	0.211	20.853	1, 18	1	0.0008
BAB 3	0.52	25.15	10.926	6.379	0.418	0.209	20.509	1, 18	1	0.0009
BAB 4	0.52	25.15	10.926	6.379	0.418	0.209	20.509	1, 18	1	0.0009
BAB 5	0.54	26.36	11.289	6.517	0.475	0.204	21.258	1, 18	1	0.0008
BAB 6	0.52	25.15	10.926	6.379	0.418	0.209	20.509	1, 18	1	0.0009
BAB 7	0.50	24.15	10.542	6.186	0.484	0.211	19.778	1, 18	1	0.0009
BAB 8	0.52	25.15	10.926	6.379	0.418	0.209	20.509	1, 18	1	0.0009
BAB 9	0.52	25.15	10.926	6.379	0.418	0.209	20.509	1, 18	1	0.0009
BAB 10	0.49	23.71	10.361	6.075	0.485	0.212	19.427	1, 18	1	0.0009
BAB 11	0.52	25.15	10.926	6.379	0.418	0.209	20.509	1, 18	1	0.0009
BAB 12	0.50	24.15	10.542	6.186	0.484	0.211	19.778	1, 18	1	0.0009
BAB 13	0.52	25.15	10.926	6.379	0.418	0.209	20.509	1, 18	1	0.0009
BAB 14	0.51	24.58	10.743	6.308	0.484	0.211	20.144	1, 18	1	0.0009
BAB 15	0.54	26.36	11.289	6.517	0.475	0.204	21.258	1, 18	1	0.0008

Table 7.2 shows the data obtained from the failure analysis of BAB symmetric samples. Table gives the information about the theoretical stiffness and failure nature of laminate structure. As an instance, for sample BAB1 the theoretical young's modulus was found to be 25.15GPa which is more than the experimental data obtained (21.950 GPa). When 1MN of force was applied on the sample

with the bending moment of per unit length of width, two plies 1^{th} and 18^{th} fails first where 0.0009 MN gives the first failure.

8 Comparison

The experimental flexural modulus, Exp. E (MPa), and theoretical flexural modulus, the.E(MPa) of the samples ABA and BAB are compared in tables below. The difference between them is analyzed with reference of number of defects in samples.

Table 8.1 Comparison for experimental and theoretical strength of ABA samples

Samples	No. of defcts	Exp.E(MPa)	The. E(MPa)	diff. E(MPa)
ABA1	1	28921.57	30605	1683.42999
ABA2	7	24864.7059	29971	5106.29408
ABA3	7	24200.8433	29971	5770.1567
ABA4	4	26605.4411	29313	2707.5589
ABA5	3	27940.5412	30605	2664.45883
ABA6	8	22705.9699	29971	7265.03011
ABA7	4	28007.9317	30605	2597.06834
ABA8	6	24650.5801	29971	5320.41988
ABA10	2	28087.0381	29971	1883.96189
ABA11	3	25944.4288	29971	4026.57123
ABA12	3	22876.9516	29313	6436.04837
ABA13	8	22638.3012	29313	6674.69876
ABA14	7	23568.5609	28919	5350.43909
ABA15	3	26338.2088	30605	4266.79119
ABA16	0	26438.2838	29313	2874.71619

Table 8.1 shows the experimental and theoretical modulus of samples ABA with the number of defects detected in them. The data shows how the defects effect the strength of samples. ABA8 has 8 detected air bubbles on the surface which is highest number of defects in one sample, experimental flexural modulus is found to be 22705.9699 MPa, where the calculation was done theoretically assuming the sample is free from defects the modulus is found to be 29971 MPa. There was difference of 7265.03 MPa between two modulus which is the highest among the data obtained. Whereas in sample ABA1 the difference between the modulus is the lowest (1683.4.3

MPa). The sample had only 1 detected air bubbles. The pattern on the table shows that with increasing number of defects on sample the experimental strength decrease.

Although, no defects were detected on sample ABA16 there's certain difference between the modulus.

Table 8.2 Comparison for experimental and theoretical strength of BAB samples

Samples	No. of defects	Exp. E(MPa)	The. E (MPa)	Diff. E (MPa)
BAB1	3	21950.2522	25148	3197.74778
BAB2	2	20847.2244	25466	4618.77563
BAB3	8	19853.3609	25148	5294.63907
BAB4	8	20209.3903	25148	4938.60967
BAB5	3	22971.3369	26360	3388.66308
BAB6	4	21729.3036	25148	3418.69637
BAB7	5	19844.0298	24145	4300.97024
BAB8	0	22788.3523	25148	2359.64773
BAB9	3	22361.5927	25148	2786.40726
BAB10	0	19145.7741	23714	4568.22592
BAB11	0	20954.8693	25148	4193.1307
BAB12	1	20425.7234	24145	3719.27662
BAB13	2	21361.3344	25148	3786.66556
BAB14	3	21243.0841	24576	3332.91589
BAB15	2	22921.8234	26360	3438.17657

From Table 8.2, Sample BAB3 has highest number of defects detected was 8. The experimental flexural modulus was found to be 19853.36 MPa, whereas theoretical calculation gave 25148 MPa. The difference between two moduli was the highest among the samples which was 5294.64 MPa. Sample BAB10 has the lowest experimental modulus (19145.77 MPa) among BAB samples. It has no detected defects on the surface. The pattern on the table somehow shows that the bending modolus of sample decreases with increasing number of defects.

9 Conclusion

The main aim of this research was to detect the surface defects on the laminate composites through microscopic analysis and study changes occurs on the specimen due to those defects. Thirty different types of glass fiber's samples composites were used for the research. Air bubbles, voids

and some other fiber impurities were detected through microscopic analysis. Air bubbles were detected in the yawns. Stress was not thoroughly distributed due to the defects possessed on the samples.

Comparing the data obtained from 3-point bending and theoretical calculation from CCSM calculator it showed that, the strength of sample is less than it was supposed to be. As the theoretical data, the samples were supposed to have certain value of flexural modulus but experimental data shows that the sample has less flexural modulus. The fact indicates that the strength of samples was reduced to some point. It concludes that the defects reduced the area of the force applied on the surface as a result the stress distribution was uneven which leads to the failure of samples before they were supposed to. it showed that with increasing number of defects on the surface, the strength of sample decrease.

I was only able to analyze top surface of the composites. The microscope could not be adjusted to analyzed the other part of the surface as the samples were cut in bigger size. There is the possibility of missing the detection of defects on the microscope analysis as only the surface of samples was analyzed the formation of crack and crack growth on the sample was not studied.

The results retrieved from the study partially fulfill the objective and expectation intended. Even though accurate values were not gathered as it was difficult to identify the defects, the final result gave the indications on the effects of surface defects on the strength of the laminate composites. Though the method for analyzing the defects might seem more economical and easy, it was not more accurate. However, the result obtained can be just a starting point for more accurate result and analysis.

10 References

[1] D. P. R. J. B. M. Zacal Jaroslav, "Analysis of Surface Defects in Composites Using Digital Correlation and Acoustic Emission," *Acta Universitatis Agriculturae et Silviculturate Mendeliande Brunensis,* vol. 66, no. 5, pp. 1217-1224, 2018.

[2] The Editor of Encyclopaedia Britannica, "Hooke's law," Encyclopaedia Britannica, 15 December 2017. [Online]. Available: https://www.britannica.com/science/Hookes-law. [Accessed 25 October 2019].

[3] toppr, "Hooke's Law and Stress-Strain Curve," toppr, [Online]. Available: https://www.toppr.com/guides/physics/mechanical-properties-of-solids/hookes-law-and-stress-strain-curve/. [Accessed 25 October 2019].

[4] P. Mishra, "Mechanical Booster," Mechanical Booster, 6 april 2017. [Online]. Available: https://www.mechanicalbooster.com/2017/04/what-is-stress-concentration.html. [Accessed 3 october 2019].

[5] Engineersedge, "Engineersedge," Engineers Edge, [Online]. Available: https://www.engineersedge.com/material_science/stress_concentration_fundamentals_9902.htm. [Accessed 3 Oct 2019].

[6] W. D. Pilkey, Peterson's Stress Concentration Fractors, 2nd ed., New York: John Wiley & Sons, 1997, p. 501.

[7] M. Y., Theory of Elasticity and Stress Concentration, 1st ed., New York: John Wiley & Sons, 2016, p. 474.

[8] G. Todd, "stress concentration on holes," [Online]. Available: https://www.fracturemechanics.org/hole.html. [Accessed 02 07 2020].

[9] D. F. P. Walter D. Pilkey, Peterson's Stress Concentration Factors, third ed., New Work: John Wiley and Sons,Inc, 2008.

[10] S. Ramsay, *Intoduction to Fracture and the Stress Concentration Factor,* YouTube, 2014.

[11] D. Roylance, "Intoduction to fracture Mechanics," Massachusetts Institute of Technology, Cambridge, 2001.

[12] R. F. Gibson, Principles of Composite Material Mechanics, 3rd ed., CRC Press LLC, 2011, p. 659.

[13] B. McGinty, "Stress Intensity Factor," oct 2014. [Online]. Available: https://www.fracturemechanics.org/sif.html#refs. [Accessed 16 oct 2019].

[14] Bruker, "3-Point Bending Testing," Bruker, [Online]. Available: https://www.bruker.com/products/surface-and-dimensional-analysis/tribometers-and-mechanical-testers/application-pages/3-point-bend-testing.html. [Accessed 5 jan 2020].

[15] "The Three Point Bend Test," [Online]. Available: http://mi.eng.cam.ac.uk/IALego/bender_files/bend_theory.pdf. [Accessed 05 jan 2020].